A shortcut to high-quality gmelinite through steam-assisted interzeolite transformation

Mielby, Jerrik; Møller, Kristoffer Hauberg; Iltsiou, Dimitra; Goodarzi, Farnoosh; Enemark-Rasmussen, Kasper; Kegnæs, Søren

Published in:
Microporous and Mesoporous Materials

Link to article, DOI:
10.1016/j.micromeso.2021.111606

Publication date:
2022

Document Version
Publisher's PDF, also known as Version of record

Microporous and Mesoporous Materials 330 (2022) 111606

Contents lists available at ScienceDirect

Microporous and Mesoporous Materials

journal homepage: www.elsevier.com/locate/micromeso

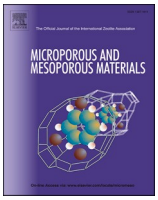

A shortcut to high-quality gmelinite through steam-assisted interzeolite transformation

Jerrik Mielby [*], Kristoffer Hauberg Møller, Dimitra Iltsiou, Farnoosh Goodarzi, Kasper Enemark-Rasmussen, Søren Kegnæs [**]

DTU Chemistry, Technical University of Denmark, Kemitorvet 207, DK-2800 Kgs, Lyngby, Denmark

A B S T R A C T

Mechanochemical activation and steam-assisted interzeolite transformation offer a simple, fast and cost-efficient synthesis route to gmelinite (GME) zeolite. The use of faujasite (FAU) as the parent zeolite precursor facilitates the reaction and results in high yields of high-quality GME in less than 20 h under optimized conditions. The accessible porosity and amounts of stacking-faults were determined by N_2 physisorption and XRD analysis, respectively. The results show that the quality of the prepared materials easily competes with GME zeolites synthesized by conventional hydrothermal synthesis, which encourages further research in this area. By changing the reaction parameters, the approach may also be used for the production of several other types of zeolites, including MOR, MFI and ANA.

1. Introduction

Zeolites are crystalline microporous aluminum-silicates that find multiple industrial applications because of their ability to ion-exchange cations and their high acidity on proton-form. The arrangements of tetrahedrally coordinated Si and Al atoms give rise to a large number of three-dimensional frameworks that have well-defined systems of pores and cages in different sizes and shapes. Because these pores are in the same dimensions as small molecules, zeolites are also known as molecular sieves. Their remarkable size- and shape-selective properties make zeolites particularly useful for gas separation and catalysis, where each zeolite framework provides a unique reaction environment that results in different catalytic properties in terms of activity, selectivity and stability.

Although more than 240 zeolites are known, and new frameworks are still frequently reported [1], the synthesis of some long-known topologies still represents a significant challenge [2]. Specifically, these syntheses often rely on complicated reaction procedures, lengthy crystallizations and the use of expensive organic structure-directing agents (OSDAs).

One such example is the zeolite gmelinite (GME), which consists of double-six-membered rings (*d6r*) and characteristic GME cages. GME has a three-dimensional multipore system with large 12-membered ring channels in one direction and small 8-membered ring channels in the two other. Like other large-pore zeolites, GME has potential applications in shape-selective catalysis and gas separation [2,3]. Unfortunately, natural and synthetic GME zeolite crystals often contain stacking faults and intergrowths with the small-pore zeolite chabazite (CHA). These stacking faults block the large 12-membered pores, which decreases the porosity and limits potential applications. Both GME and CHA consist of stacked layers of *d6r*, where each layer rotates 60° relative to the previous layer. For the GME structure, the rotation occurs in alternate directions (AABB … sequence), while for CHA, the rotation consistently occurs in the same direction (AABBCC … sequence) [4]. Because of this structural similarity, stacking-faults and other crystalline disorders such as intergrowths and epitaxial overgrowths are often present in GME zeolites.

Several research groups have devoted much effort to developing high-quality CHA-free GME, both with and without OSDAs [5]. Recently, Dusselier et al. [2] managed to synthesize completely fault-free GME using an enantiomeric pure *N,N*-dimethyl-3,5-dimethylpiperidinium hydroxide in the *cis*-form after 110 h at 140 °C. Since the GME structure is unstable at high temperatures and cannot be calcined, the researchers treated the materials with ozone for 24 h at 150 °C to remove the OSDA. The resulting GME material (named CIT-9) had an unprecedented total pore volume of 0.17 cm^3/g. In contrast, the template-free synthesis of GME zeolites typically relies on interzeolite transformations. In 1999, Chiyoda and Davis [6] reported the synthesis of GME starting from Sr-exchanged FAU. The transformation occurred in a synthesis medium containing $SrCl_2$ and took 14 days at 240 °C. More

* Corresponding author.
** Corresponding author.
E-mail addresses: jjmie@kemi.dtu.dk (J. Mielby), skk@kemi.dtu.dk (S. Kegnæs).

https://doi.org/10.1016/j.micromeso.2021.111606
Received 30 August 2021; Received in revised form 25 November 2021; Accepted 28 November 2021
Available online 1 December 2021

recently, Xie [7] patented the synthesis of GME starting from FAU using NaOH in conventional hydrothermal synthesis. The GME formed within 4–5 days at 125 °C.

One particular advantage of interzeolite transformations over conventional hydrothermal synthesis is the crystallization rate. Sano and co-workers [8] studied several interzeolite transformations and showed that using FAU as the parent zeolite increased the crystallization rate compared to the conventional synthesis starting from amorphous aluminosilicate precursors. The researchers explained the high rate by the presence of small fragments of ordered aluminosilicate species (nanoparts) that form by the decomposition of the parent zeolite. Similar explanations were also given by Iglesia and co-workers [9], who studied the OSDA-free transformations of BEA into MFI and FAU into CHA. Since interzeolite transformations are dictated by thermodynamics and kinetics, the researchers argued that the common building units or seeds of the target zeolite direct the synthesis by overcoming kinetic barriers.

FAU is readily available and often used as parent zeolite because it has a relatively low framework density (FD_{Si} = 13.3), which gives a thermodynamic advantage during the interzeolite transformation. In general, the increase in framework density agrees well with Ostwald's step rule – a commonly observed phenomenon in which multiple metastable phases crystallize sequentially until reaching a stable phase. Therefore, FAU has previously found use as parent zeolite in the synthesis of CHA [9–15], AEI [16], AFX [17], BEA [8], LEV [8], ERI [18], STW [9], MER [13], MOR [19], ABW [13], MTW [9], MFI [9], ANA [13] (FD_{Si} = 15.1–19.2) and many more. Interestingly, FAU shares secondary building units with some of these frameworks, but not all, demonstrating the versatility of using FAU as the starting material.

Here, we present a fast and cost-efficient synthesis of high-quality GME by mechanochemical activation and steam-assisted interzeolite transformation. In the first step of the synthesis, zeolite FAU is thoroughly ground with NaOH in a mortar. In the second step, the semi-dry material transforms into GME zeolite under steam-assisted conditions. The synthesis needs no expensive OSDAs and only a small amount of water to generate saturated steam inside the autoclave. Since FAU zeolite is already produced without OSDAs on a large scale, the method potentially provides an all organic-free synthesis route to high-quality GME. Compared to conventional hydrothermal synthesis, where the aluminum silicate precursors are dissolved in a highly diluted gel, the steam-assisted synthesis results in faster crystallization, less liquid waste, higher yields, and better exploitation of the autoclave volume [20–23]. For these reasons, the steam-assisted method holds great potential for large-scale production.

2. Results

The Si/Al ratio, the Na/Si ratio, the temperature, and the crystallization time are well-known to affect the outcome of an interzeolite transformation. By changing these parameters, we found that it was possible to grind FAU with NaOH and convert the resulting material into several different zeolite framework types, including MOR, MFI, ANA, and GME. Fig. 1 show an outline of the key results.

Under appropriate conditions, we also found that FAU converted into a high amount of GME. These results encouraged us to optimize the reaction conditions and perform a more detailed investigation of the individual synthesis parameters. In the first set of experiments, we added different NaOH amounts to change the Si/Na ratio from 1.5 to 3.0 (labeled 1.5–3.0_GME, respectively). The XRD patterns in Fig. 2 show characteristic peaks from FAU at a Si/Na ratio above 2.2, which showed that FAU did not fully convert into GME under these conditions. At Si/Na ratios below 2.2, the XRD patterns showed a peak at 2θ = 15.9°, which we attribute to CHA intergrowths. Fig. 2 also shows that the amount of CHA intergrowths increases as the Si/Na ratio decreased from 1.9 to 1.5. Only at a Si/Na ratio of 2.2 did the XRD pattern show no peaks from FAU or CHA. However, detailed examination and Rietveld refinement of the XRD patterns in Fig. 2 did reveal a small impurity from the

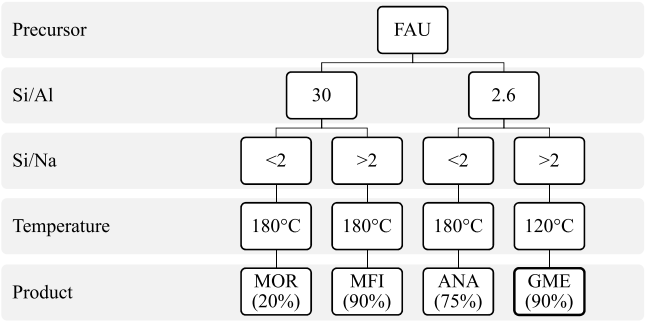

Fig. 1. Decision tree showing the key results from our initial investigations of the mechanochemical activation and steam-assisted interzeolite transformation of FAU after 20 h. Yields are given in weight percentages.

GIS polymorph Na-P2 at 2θ = 28.04°. GIS is an 8-membered small pore zeolite that is well-known to form during the hydrothermal transformation of FAU in aqueous solutions of NaOH [24]. With a Si/Al ratio of 2.6 and a Si/Na ratio of 2.2, the relative molar composition of Si:Al:NaOH is around 0.54:0.21:0.25. Compared to the kinetic ternary phase diagrams previously reported by Rimer and co-workers [25], this composition is in the Si-rich region (Si/Al>1) that does not form GIS. Therefore, we speculate that the inhomogeneous distribution of NaOH in the solid gel could explain the GIS impurity.

Figure S1 shows the SEM images of 2.2_GME and 1.5_GME, respectively. The images show that the hexagonal GME crystal varied significantly in size and shape. In general, the GME was quite different from the smaller FAU crystals, which made it possible to follow the interzeolite conversion by SEM. As expected from the XRD analysis, a detailed examination of the SEM images revealed a small number of larger crystals with the characteristic GIS morphology [24].

With the Si/Na ratio kept at 2.2, we then studied the effect of the temperature. Fig. 3 shows the XRD patterns of the products obtained after 20 h at 100–140 °C. The patterns show that the peaks from unconverted FAU were still present at 110 °C, while peaks related to CHA intergrowth started to appear at 130 °C. In general, the increased temperature did not result in any significant changes in the crystal morphology.

Figure S2 the XRD patterns of samples collected after crystallization for 2–20 h at 120 °C (Si/Al = 2.6 and Si/Na = 2.2). After 2 h, the XRD shows all the characteristic peaks for FAU. After 6 h, the FAU started to convert into GME, and new peaks appeared in the diffractogram. The amount of GME continued to increase at the expense of the FAU precursor until after 20 h, where the interzeolite transformation appeared to be complete. While the small impurity from GIS appeared throughout the crystallization process, the XRD and SEM analysis did not indicate that any amorphous phase formed during the interzeolite transformation. Therefore, we speculate that our washing procedure could remove some soluble species other than NaOH. However, considering the limited amount of water and relatively high concentration of precursors, another explanation could also be that the reorganization of double 6-membered rings and the crystallization of GME is faster than the dissolution of FAU. At this point, the intimate mechanistic details of the interzeolite transformation under steam-assisted conditions are still not fully understood.

The SEM images in Fig. 4 confirm that no hexagonal GME crystals are present after 2 h. As expected from the XRD, we observed the first GME crystals after 6 h. The number of GME crystals increases with the crystallization time, and their size typically varies between 1 and 4 μm.

Fig. 5 shows the results from the ^{29}Si solid-state NMR analysis of the materials compared to a reference NaY sample with a Si/Al ratio of 2.6. The NMR spectrum of the FAU precursor, which was mainly on the H-form, showed four distinct peaks and one small shoulder, which corresponds to the five possible Q^4(mAl) sites. After 2 h, the NMR spectrum

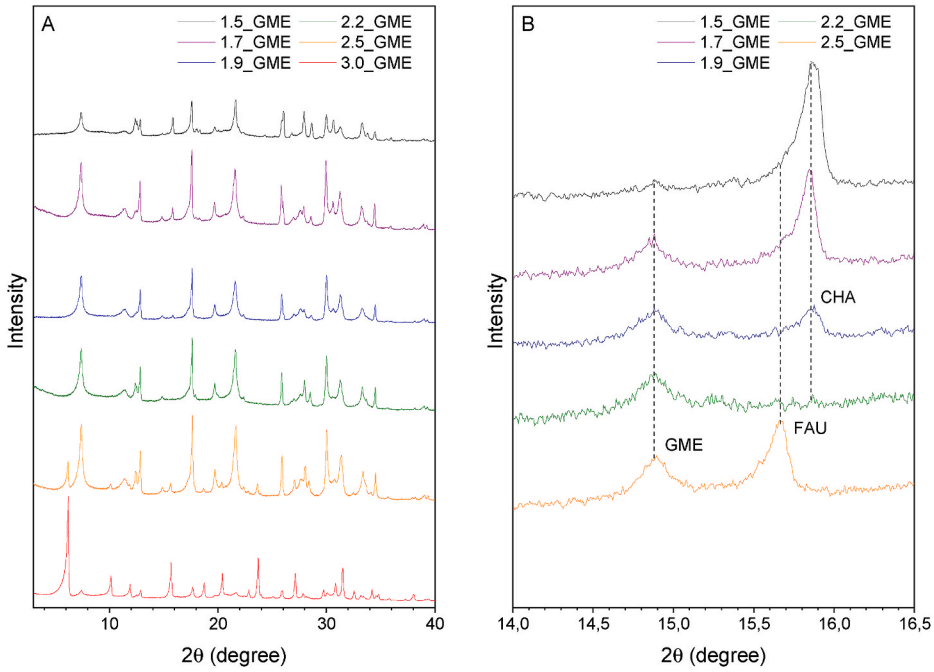

Fig. 2. A) XRD patterns of GME zeolites prepared with Si/Al = 2.6 and Si/Na ranging from 1.5 to 3.0 after 20 h at 120 °C. B) Close-up of the XRD showing characteristic diffraction peaks from GME (weak), FAU and CHA.

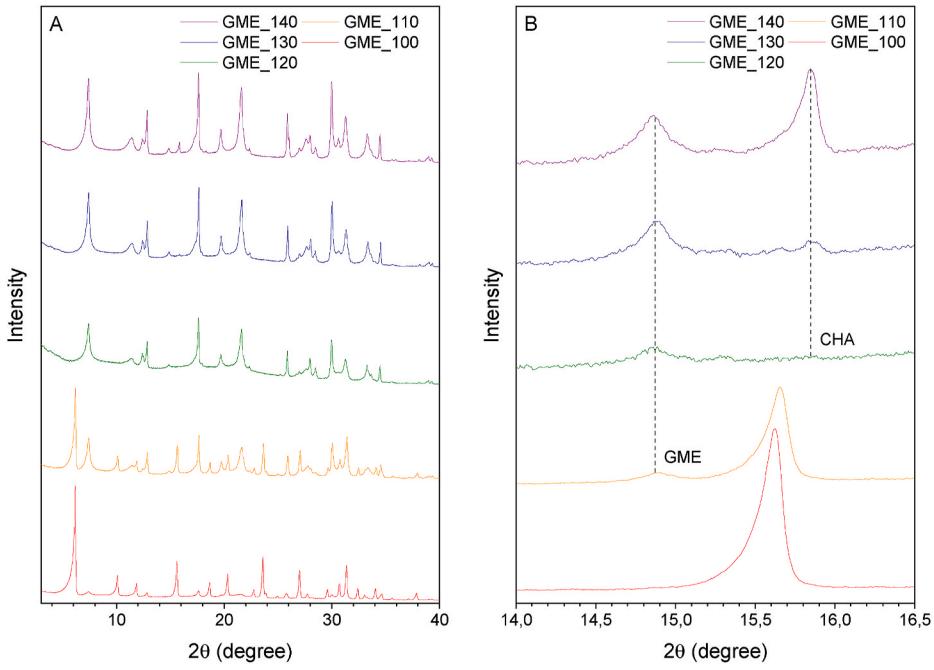

Fig. 3. A) XRD patterns of GME zeolites prepared with Si/Al = 2.6, Si/Na = 2.2 and temperatures ranging from 100 to 140 °C. B) Close-up of the XRD showing characteristic diffraction peaks from GME (weak), FAU and CHA.

resembled that of the NaY reference, which indicated that the extra-framework material was converted and that the zeolite was ion-exchanged with Na. As expected from XRD and SEM, the NMR analysis did not reveal any GME in this sample. After 6 h, the NMR peaks from FAU and GME started to overlap. A simulation of the overlap showed that around 40% of the FAU was converted at this point. After 12 and 20 h, the NMR spectra were quite similar, although the relative peak intensities indicated a slight increase in the Si/Al ratio.

From the Si/Al ratios, we also calculated the relative intensity of the different Q^n(mAl) sites expected from a random Al distribution that obeys Löwenstein's rule [26]. The data in Table S3 show that the relative intensity of the Q^4(2Al) sites is higher than predicted. The data also show that Si/Al ratio of the GME increased with the crystallization time, which resulted in more Q^4(1Al) sites and less Q^4(3Al) and Q^4(4Al) sites.

Fig. 6 shows the results from ^{27}Al solid-state NMR analysis. All peak positions and FWHM values are listed in the supporting information, Table S2. The NMR of the NaY reference only showed one peak at 63 ppm, which corresponds to the tetrahedral coordinated framework Al. The FAU precursor spectrum had 4 peaks, which is typical for ultra-stable Y zeolites prepared by high-temperature steaming [27]. While

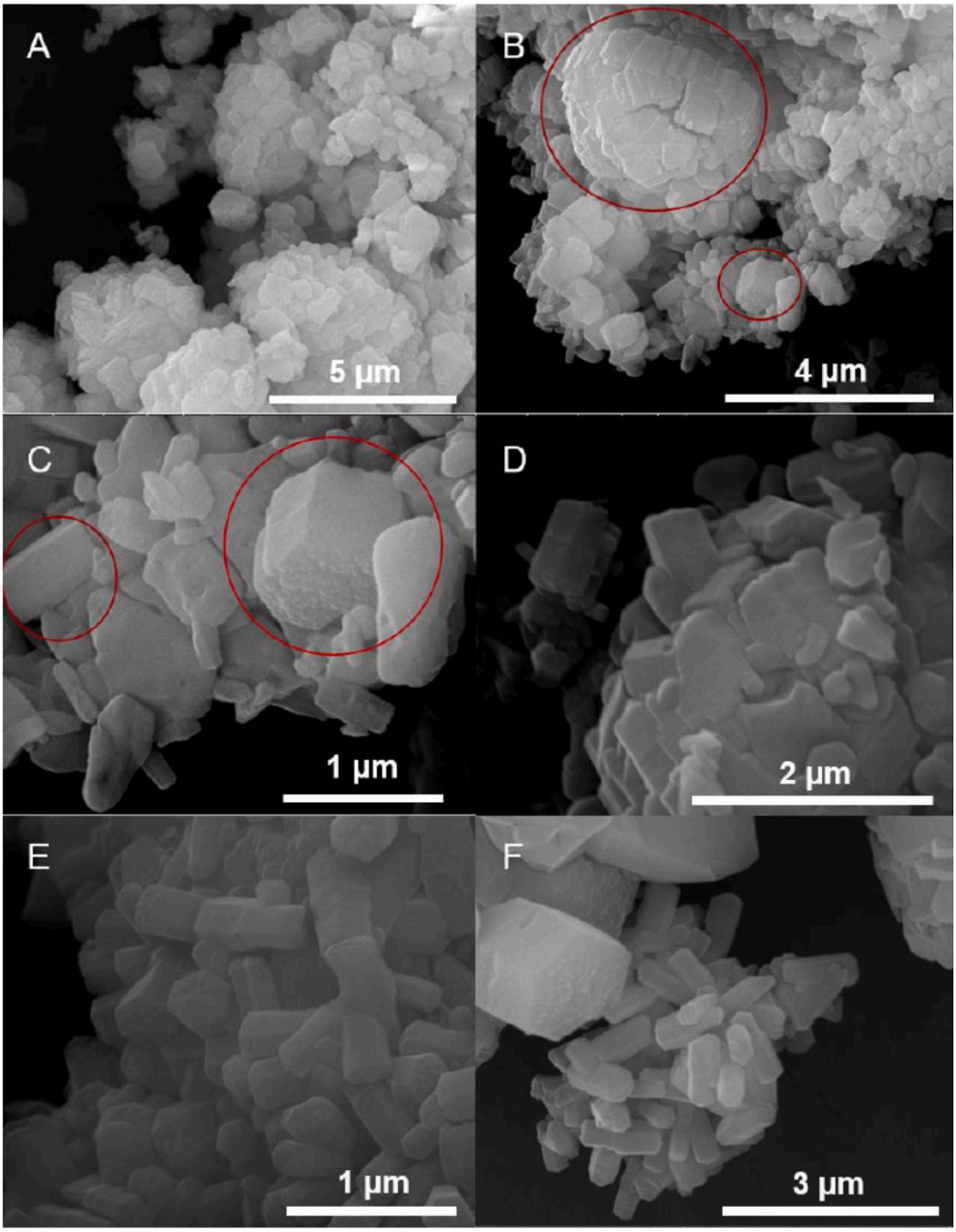

Fig. 4. SEM images of GME_2h (A), GME_6h (B + C), GME_12h (D), GME_15h (E) and GME_20h (F) prepared with Si/Al = 2.6, Si/Na = 2.2 and at 120 °C. Red circles mark typical GME shaped crystals. (For interpretation of the references to colour in this figure legend, the reader is referred to the Web version of this article.)

the two peaks at 62 and 54 ppm are attributed to tetrahedral coordinated framework Al, the peak at 35 and 3 ppm are attributed to penta- and octahedral coordinated extra-framework species, respectively.

Furthermore, we attribute the broad tetrahedral peak to species, which are in close vicinity to defects or cationic extra-framework Al [28]. After 2 h in the autoclave, all of the Al had shifted into the tetrahedral position at 63 ppm. This shift indicates that a significant reorganization of the extra-framework Al occurs at the beginning of the crystallization process. Compared to the NaY reference, the tetrahedral peak was broader (larger FWHM), which indicated a higher degree of disorder in the framework. After 6 and 12 h, the tetrahedral Al peak shifted to 62.3 and 61.6 ppm, respectively. After 20 h, the FWHM decreased from 580 to 550 Hz, which indicated that the degree of order increased with the crystallization time.

The increasing crystalline order encouraged us to extend the crystallization time. Figure S3 shows the XRD analysis of the samples collected after 24, 30, 36, 40 and 46 h, respectively. In general, the diffraction patterns were quite similar, although the small impurity of GIS seemed to increase with time.

Table 1 compiles all results from the N_2 physisorption analysis. Entries 1–3 show the results of the GME zeolites prepared by decreasing the Si/Na ratio. As expected from the XRD, a high amount of NaOH resulted in a high amount of CHA intergrowths and, consequently, a relatively limited surface area and porosity. Increasing the temperature to 130 °C and 140 °C (entry 4-5) resulted in CHA intergrowth and higher adsorption of N_2. It is unclear if the increased porosity was caused by a

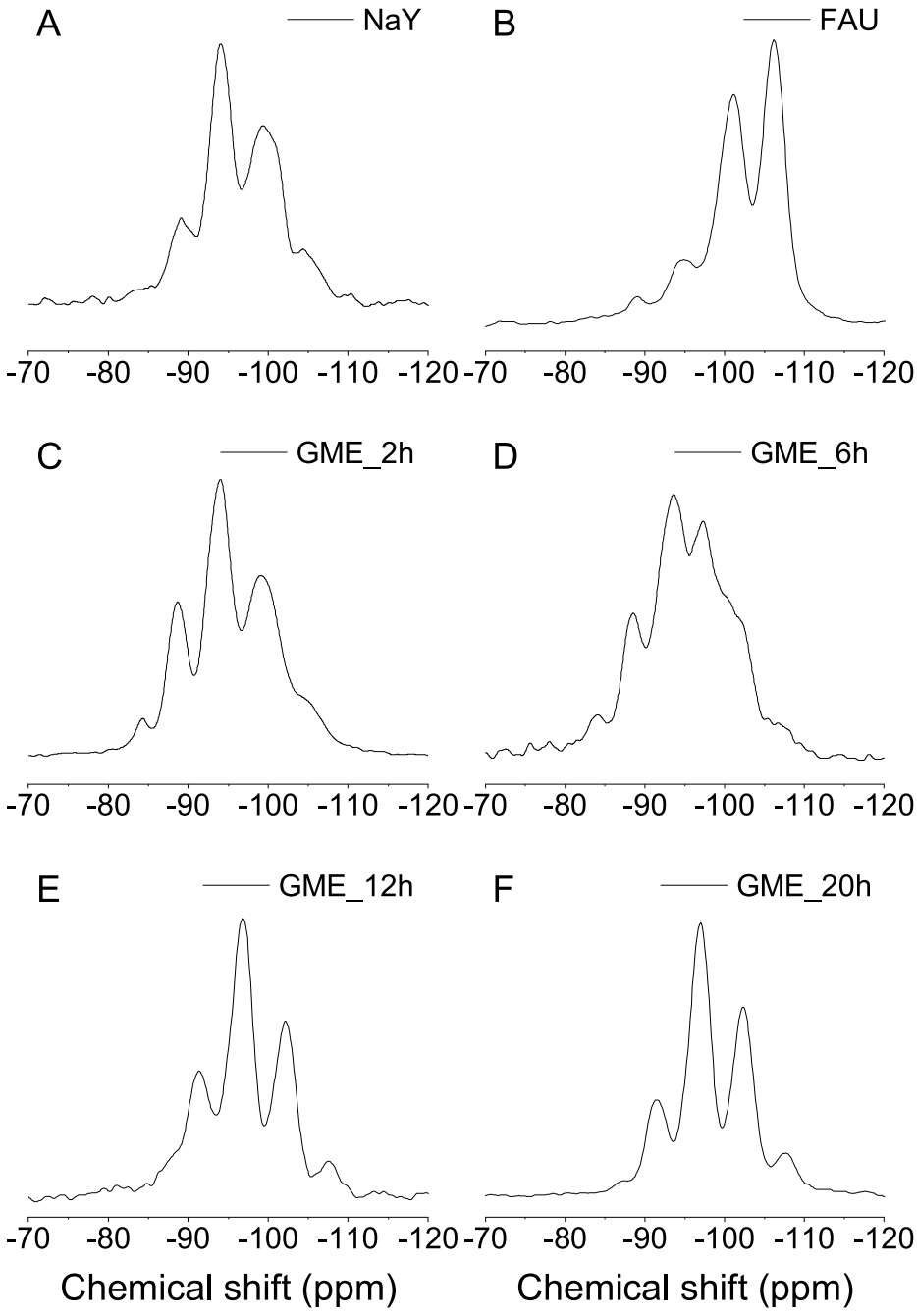

Fig. 5. ^{29}Si MAS NMR spectra of A) NaY, B) FAU, C) GME_2h, D) GME_6h, E) GME_12h and F) GME_20h.

higher crystallinity or less GIS formation. As expected from the NMR analysis, prolonging the crystallization time resulted in higher crystalline order with increasing pore accessibility. After 46 h at 120 °C, the total pore volume was 0.13 cm^3/g. This porosity is significantly higher than Na-GME synthesized from Sr-FAU, which has a total porosity of 0.03 cm^3/g [29]. More recently, Xie [7] achieved a total pore volume of 0.12 cm^3/g from a similar interzeolite transformation under conventional hydrothermal synthesis conditions.

To estimate the amount of CHA-stacking faults in the prepared materials, we simulated a series of XRD patterns with an increasing probability for disorders in the AABB-sequence. The simulations were performed in GSASII using a suite of subroutines from the DiFFAX program developed by Treacy et al. [30] We used the *d6r* as the periodic building unit and constructed the AB-plane from the CIF file, which is available from the international zeolite association. A detailed description of the layer, the lattice parameters, and the layer-layer transitions are given in the supporting information. Based on a direct comparison of the observed diffraction patterns with the simulated data in Figure S4, we estimate that the prepared zeolites contained less than around 5% CHA stacking faults.

3. Conclusions

In conclusion, we have shown that mechanochemical activation and steam-assisted interzeolite transformation offer a simple, fast and cost-efficient alternative to conventional hydrothermal synthesis of GME. The synthesis uses FAU as the parent zeolite precursor, which potentially provides an organic-free synthesis route that has great potential for large-scale production. High yields of high-quality GME can be achieved in less than 20 h at 120 °C, although longer crystallization times increase

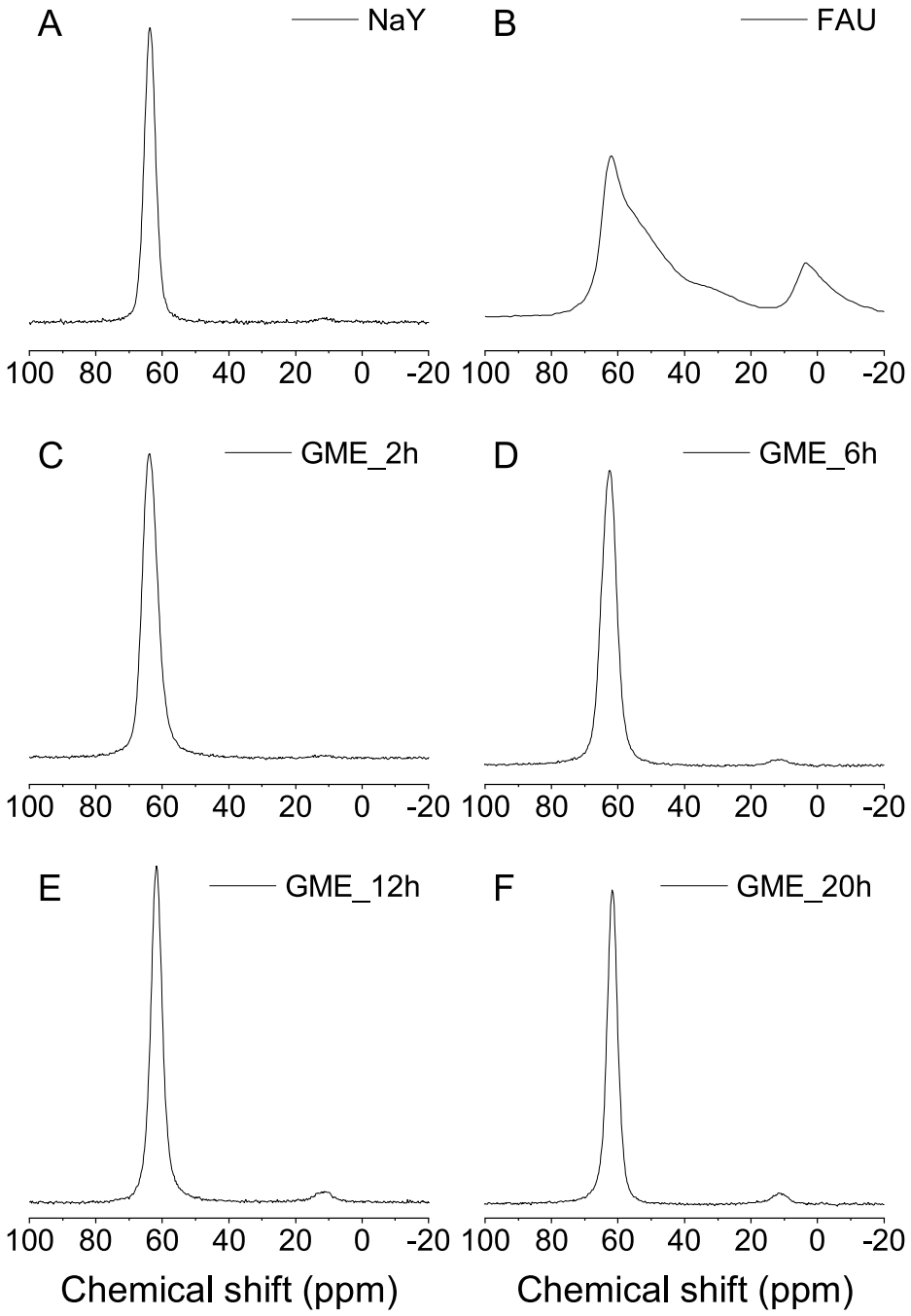

Fig. 6. ^{27}Al MAS NMR spectra of A) NaY, B) FAU, C) GME_2h, D) GME_6h, E) GME_12h and F) GME_20h. Small peaks around 11 ppm in D-F are from spinning sidebands.

the crystallinity and pore accessibility. We note that a range of different frameworks can be synthesized under similar steam-assisted conditions and expect that more insight into the transformation mechanism may provide a better-directed synthesis of zeolites with minimal environmental impact.

4. Experimental section

4.1. Materials and chemicals

H(Na)-Y type FAU (CBV400, Si/Al = 2.55) and Na-Y (CBV100, Si/Al = 2.55) were purchased from Zeolyst and used without further purification or pretreatment. Sodium hydroxide (NaOH, >99%) were purchased from Sigma-Aldrich/Merck.

4.2. Synthesis of GME

The synthesis of GME was performed by grinding 1.00 g of FAU (CBV400, Si/Al = 2.6) with 0.23 g of NaOH (Si/Na = 2.2) for 15 min in 80 ml agate mortar. The ground material was then transferred to a small Teflon beaker and put inside a 200 ml Teflon-lined autoclave containing 15 ml of H_2O. The autoclave was sealed and heated at 120 °C for 20 h. In this way, the solid gel was separated from the water until it formed saturated steam. Without water, the interzeolite transformation did not occur. Finally, the product was washed with water until neutral pH and then dried overnight at 80 °C. We investigated the effect of the Si/Na ratio in the range of 1.5–3.0 by changing the amount of NaOH. Similarly, we investigated the impact of temperature from 110 to 140 °C and the crystallization time from 2 to 48 h. The samples were assigned by the Si/

Table 1
Results from the N_2 physisorption analysis at 77 K.

Entry	Si/Na	Temp. (°C)	Time (h)	V_{micro} (cm^3/g)[a]	V_{total} (cm^3/g)[b]	S_{BET} (cm^2/g)
1	2.2	120	20	0.06	0.07	114
2	1.9	120	20	0.05	0.06	101
3	1.5	120	20	0.01	0.01	18
4	2.2	130	20	0.08	0.10	149
5	2.2	140	20	0.07	0.09	166
6	2.2	120	24	0.06	0.08	121
7	2.2	120	30	0.06	0.09	135
8	2.2	120	36	0.07	0.10	169
9	2.2	120	40	0.08	0.12	195
10	2.2	120	46	0.09	0.13	213

[a] Calculated from the t-plot.
[b] Calculated from a single point read at $p/p^\circ = 0.95$.

Na ratio followed by GME and the crystallization temperature/time (*e.g.* 2.2_GME_120C/20h). The yield was typical >90% by weight.

The synthesis conditions for MOR, MFI, and ANA were not optimized.

4.3. Characterizations

All zeolites were characterized by powder X-ray diffraction (XRD) using a Huber G670 diffractometer operated in transmission mode with Cu Kα1 irradiation from a focusing quartz monochromator. Scanning electron microscopy (SEM) analysis was performed on a FEI Quanta 200 ESEM FEG operated at 20 kV. The N2 physisorption was performed at 77 K on a 3FLEX surface area and porosimetry analyzer from Micromeritics. Before analysis, the samples were outgassed under vacuum at 400 °C overnight. The specific surface area (S_{BET}) was calculated by the Brunauer Emmett Teller method in the partial pressure range of 0.05–0.30. The micropore volumes (V_{micro}) were determined from the t-plot and the total pore volume (V_{total}) was calculated from the amount of adsorbed nitrogen at $P/P^\circ = 0.95$. The ^{27}Al and ^{29}Si MAS NMR spectra were recorded on a Bruker AVANCE III HD spectrometer operating at a magnetic field of 14.05 T equipped with a 4 mm CP/MAS BBFO probe. The ^{27}Al MAS NMR spectra were acquired with the one-pulse experiment using a 0.4 μs π/12 excitation pulse and an interscan delay of 0.5 s and the ^{29}Si MAS NMR spectra were acquired using a 4.75 μs π/2 pulse and an interscan delay of 45 s. For both ^{27}Al and ^{29}Si MAS NMR spectra, the spinning frequency was 15 kHz. High-power 1H decoupling was employed during acquisition. Peak simulations were performed with the Solids Lineshape Analysis (SOLA) module within Topspin. The ^{27}Al and ^{29}Si NMR chemical shifts were referenced to 1.0 M aqueous $AlCl_3$ ($\delta = 0$ ppm) and TMS ($\delta = 0$ ppm), respectively.

Declaration of competing interest

The authors declare that they have no known competing financial interests or personal relationships that could have appeared to influence the work reported in this paper.

Acknowledgements

The authors gratefully acknowledge the support of from the Independent Research Fund Denmark (grant no. 6111-00237), the Villum Foundation (grant no.13158) and from Haldor Topsøe A/S. The solid-state NMR spectra were recorded at the DTU NMR Center supported by the Villum Foundation.

Appendix A. Supplementary data

Supplementary data to this article can be found online at https://doi.org/10.1016/j.micromeso.2021.111606.

References

[1] Database of zeolite structures, (n.d.). http://www.iza-structure.org/databases/(accessed December 16, 2020).
[2] M. Dusselier, J.H. Kang, D. Xie, M.E. Davis, CIT-9: a fault-free gmelinite zeolite, Angew. Chem. Int. Ed. 56 (2017) 13475–13478, https://doi.org/10.1002/anie.201707452.
[3] D. Xie, H.S. Lacheen, Separation of Gases Using GME Framework Type Zeolites, 2016. US Patent 9364782.
[4] C. Baerlocher, L.B. McCusker, The ABC-6 Family, Zeolite Database, 2021. http://www.iza-structure.org/databases/.
[5] R.H. Daniels, G.T. Kerr, L.D. Rollmann, Cationic polymers as templates in zeolite crystallization, J. Am. Chem. Soc. 100 (1978) 3097–3100, https://doi.org/10.1021/ja00478a024.
[6] O. Chiyoda, M.E. Davis, Hydrothermal conversion of Y-zeolite using alkaline-earth cations 32 (1999) 257–264.
[7] D. Xie, Synthesis of GME Framework Type Zeolites, 2017. US Patent 9643853.
[8] K. Honda, A. Yashiki, M. Itakura, Y. Ide, M. Sadakane, T. Sano, Influence of seeding on FAU-BEA interzeolite conversions, Microporous Mesoporous Mater. 142 (2011) 161–167, https://doi.org/10.1016/j.micromeso.2010.11.031.
[9] S. Goel, S.I. Zones, E. Iglesia, Synthesis of zeolites via interzeolite transformations without organic structure-directing agents, Chem. Mater. 27 (2015) 2056–2066, https://doi.org/10.1021/cm504510f.
[10] Y. Ji, M.A. Deimund, Y. Bhawe, M.E. Davis, Organic-free synthesis of CHA-type zeolite catalysts for the methanol-to-olefins reaction, ACS Catal. 5 (2015) 4456–4465, https://doi.org/10.1021/acscatal.5b00404.
[11] T. Takata, N. Tsunoji, Y. Takamitsu, M. Sadakane, T. Sano, Nanosized CHA zeolites with high thermal and hydrothermal stability derived from the hydrothermal conversion of FAU zeolite, Microporous Mesoporous Mater. 225 (2016) 524–533, https://doi.org/10.1016/j.micromeso.2016.01.045.
[12] N. Martín, M. Moliner, A. Corma, High yield synthesis of high-silica chabazite by combining the role of zeolite precursors and tetraethylammonium: SCR of NOx, Chem. Commun. 51 (2015) 9965–9968, https://doi.org/10.1039/c5cc02670a.
[13] L. Van Tendeloo, E. Gobechiya, E. Breynaert, J.A. Martens, C.E.A. Kirschhock, Alkaline cations directing the transformation of FAU zeolites into five different framework types, Chem. Commun. 49 (2013) 11737–11739, https://doi.org/10.1039/c3cc47292b.
[14] K.H. Rasmussen, J. Mielby, S. Kegnaes, Towards encapsulation of nanoparticles in chabazite through interzeolite transformation, ChemCatChem 10 (2018) 4380–4385, https://doi.org/10.1002/cctc.201800914.
[15] K.H. Møller, M. Debost, L. Lakiss, S. Kegnæs, S. Mintova, Interzeolite conversion of a micronsized FAU to a nanosized CHA zeolite free of organic structure directing agent with a high CO2capacity, RSC Adv. 10 (2020) 42953–42959, https://doi.org/10.1039/d0ra04937a.
[16] J. Zhang, Y. Chu, F. Deng, Z. Feng, X. Meng, F.S. Xiao, Evolution of D6R units in the interzeolite transformation from FAU, MFI or *bEA into AEI: transfer or reassembly? Inorg. Chem. Front. 7 (2020) 2204–2211, https://doi.org/10.1039/d0qi00359j.
[17] T. Yoshioka, Z. Liu, K. Iyoki, A. Chokkalingam, Y. Yonezawa, Y. Hotta, R. Ohnishi, T. Matsuo, Y. Yanaba, K. Ohara, T. Takewaki, T. Sano, T. Okubo, T. Wakihara, Ultrafast and continuous-flow synthesis of AFX zeolite via interzeolite conversion of FAU zeolite, React. Chem. Eng. (2020), https://doi.org/10.1039/d0re00219d.
[18] X. Zhang, Y. Wang, X. Wang, H. Chen, H. Li, C. Sun, L. Sun, C. Fan, C. Wang, An efficient route for synthesis of ERI zeolite through conversion of FAU zeolite in the presence of N,N-dimethylpiperidinium hydroxide, Microporous Mesoporous Mater. 279 (2019) 407–415, https://doi.org/10.1016/j.micromeso.2019.01.021.
[19] W. Qin, R. Jain, F.C. Robles Hernández, J.D. Rimer, Organic-free interzeolite transformation in the absence of common building units, Chem. Eur J. 25 (2019) 5893–5898, https://doi.org/10.1002/chem.201901067.
[20] J. Mei, A. Duan, X. Wang, A brief review on solvent-free synthesis of zeolites, Materials (Basel) 14 (2021) 1–13, https://doi.org/10.3390/ma14040788.
[21] Q. Wu, X. Meng, X. Gao, F.S. Xiao, Solvent-free synthesis of zeolites: mechanism and utility, Acc. Chem. Res. 51 (2018) 1396–1403, https://doi.org/10.1021/acs.accounts.8b00057.
[22] J.O. Abildstrøm, M. Kegnæs, G. Hytoft, J. Mielby, S. Kegnæs, Synthesis of mesoporous zeolite catalysts by in situ formation of carbon template over nickel nanoparticles, Microporous Mesoporous Mater. 225 (2016) 232–237.
[23] H. Rasmussen, F. Goodarzi, D.B. Christensen, J. Mielby, Stabilization of metal nanoparticle catalysts via encapsulation in mesoporous zeolites by steam-assisted recrystallization, ACS Appl. Nano Mater. (2019), https://doi.org/10.1021/acsanm.9b02205.
[24] M.D. Oleksiak, A. Ghorbanpour, M.T. Conato, B.P. McGrail, L.C. Grabow, R. K. Motkuri, J.D. Rimer, Synthesis strategies for ultrastable zeolite GIS polymorphs as sorbents for selective separations, Chem. Eur J. 22 (2016) 16078–16088, https://doi.org/10.1002/chem.201602653.
[25] M. Maldonado, M.D. Oleksiak, S. Chinta, J.D. Rimer, Controlling crystal polymorphism in organic-free synthesis of na-zeolites, J. Am. Chem. Soc. 135 (2013) 2641–2652, https://doi.org/10.1021/ja3105939.
[26] C. Schroeder, M.R. Hansen, H. Koller, Ultrastabilization of zeolite Y transforms brønsted–brønsted acid pairs into brønsted–lewis acid pairs, Angew. Chem. Int. Ed. 57 (2018) 14281–14285, https://doi.org/10.1002/anie.201808395.
[27] C.A. Fyfe, J.L. Bretherton, L.Y. Lam, Solid-state NMR detection, characterization, and quantification of the multiple aluminum environments in US-Y catalysts by 27Al MAS and MQMAS experiments at very high field, J. Am. Chem. Soc. 123 (2001) 5285–5291, https://doi.org/10.1021/ja003210k.

[28] N. Malicki, G. Mali, A.A. Quoineaud, P. Bourges, L.J. Simon, F. Thibault-Starzyk, C. Fernandez, Aluminium triplets in dealuminated zeolites detected by 27Al NMR correlation spectroscopy, Microporous Mesoporous Mater. 129 (2010) 100–105, https://doi.org/10.1016/j.micromeso.2009.09.003.

[29] O. Chiyoda, M.E. Davis, Adsorption studies with gmelinite zeolites containing mono-, di- and tri-valent cations, Microporous Mesoporous Mater. 38 (2000) 143–149, https://doi.org/10.1016/S1387-1811(99)00287-5.

[30] M.M.J. Treacy, J.M. Newsam, M.W. Deem, A general recursion method for calculating diffracted intensities from crystals containing planar faults, Proc. Roy. Soc. Lond. A. 433 (1991) 499–520, https://doi.org/10.1098/rspa.1991.0062.